ELSEVIER

Catalysis Today 59 (2000) 75–86

CATALYSIS TODAY

www.elsevier.com/locate/cattod

Experimental and numerical studies on combustion characteristics of a catalytically stabilized combustor

Yong Seog Seo [a,*], Sung June Cho [a], Sung Kyu Kang [a], Hyun Dong Shin [b]

[a] *Korea Institute of Energy Research, 71-2 Jang-dong Yusung-gu, Taejon, 305-343, South Korea*

[b] *Korea Advanced Institute of Science and Technology, 373-1 Kusong-dong Yusong-gu, Taejon, South Korea*

Abstract

This study aims to investigate surface catalytic reaction and flame combustion of lean premixed mixture in a catalytically stabilized combustor through experiment and modeling. Five types of catalyst beds composed of various combinations of noble metal catalysts, Pd and Pt, and a high temperature catalyst, La–Mn–hexaaluminate, were tested. Results showed that the most active catalyst system consisted of a Pd catalyst in the first stage of the catalyst bed and a Pt catalyst in the second stage. A numerical simulation, consisting of three sets of multi-step elementary surface reactions for CH_4 oxidation over Pt, was conducted and the most accurate model was used to evaluate the catalyst bed and the homogeneous reaction. The numerical simulation showed that the flame speed of the mixture supported by catalytic surface reaction was much raised as compared to the mixture without a catalytic combustion.

Keywords: Catalytic combustion; Catalyst bed; Thermal combustor; Hexaaluminate; Flame ignition; Modeling; Multi-step surface reaction; Pd; Pt

1. Introduction

Catalytic combustion has been studied to develop ultra low NO_x combustion technology for the last two decades. One application of catalytic combustion is a gas turbine combustor. For this purpose, various design concepts have been developed. Sadamori et al. [1] have developed a catalytic combustor in which the entire mixture of fuel and air is combusted within the catalyst bed. Temperatures of a catalyst bed were reported to increase up to the adiabatic flame temperature of mixture, about 1300°C, and the high temperature catalyst of hexaaluminate was used.

Furuya et al. [2] reported a catalytic combustor consisting two parts — the catalyst bed and the thermal combustor. A fraction of the fuel and all of combustion air enter the catalyst bed, and the rest of fuel is introduced to the thermal combustor placed at the downstream of the catalyst bed. This has been called a hybrid catalytic combustor. An advantage of this concept is that temperatures of the catalyst bed remain below 1000°C. This enables the existing catalysts to be reliably used. However, since the gas nozzle is placed in the thermal combustor, non-uniform mixing of fuel and air may produce hot spots and emit very high levels of thermal NO_x.

Dalla Betta et al. [3,4] have developed another type of catalytic combustor in which the entire mixture of fuel and combustion air is introduced to the catalyst bed. Only a fraction of fuel is combusted in the catalyst bed and the unburned fuel is combusted in the thermal combustor placed at the downstream of the catalyst bed. The catalyst plays a role of supporting

* Corresponding author.
E-mail address: ysseo@kier.re.kr (Y.S. Seo)

0920-5861/00/$ – see front matter
PII: S0920-5861(00)00274-1

flame combustion of the mixture in the thermal combustor. This concept has been called CST (catalytically stabilized or supported thermal) combustor. This design was proposed by Pefferle [5] for the first time and has been studied by many other researchers [6–9].

The present work focused on a numerical and experimental investigation of the CST combustor using LNG (liquefied natural gas) at atmospheric pressure. We tested five types of the catalyst beds composed of Pt, Pd and La–Mn–hexaalumiate. First, the behavior of each catalyst bed was investigated at various mixture velocities, preheating temperatures, and fuel concentrations. Light-off temperatures and temperature distributions within each catalyst bed were analyzed. Secondly, flame ignition in the thermal combustor was investigated for each catalyst bed at various operating conditions.

A numerical simulation of the catalytic combustor was also performed to examine how the surface reaction affects the gas reaction in a catalytically stabilized combustor. To model the catalytic combustor, a multi-step surface reaction on CH_4 oxidation over Pt catalyst was used together with a multi-step gas reaction.

2. Experimental

Pd and Pt catalysts were supported on ceramic honeycomb consisting of 50% codierite and 50% mullite with a cell size of 300 cells/in^2. The honeycomb was washcoated with 20 wt.% γ-alumina of high surface area, $\sim$100 m^2/g. Catalysts were then added to the washcoated honeycomb by impregnation with aqueous palladium nitrate ($Pd(NO_3)_2$) (19.96% Pd, Engelhard) for the Pd catalyst and hexachloroplatinatic acid (H_2PtCl_6) (40.0% Pt, Engelhard) for the Pt catalyst. The catalysts were dried at 100°C for 12 h and calcined at 550°C for 6 h. The catalyst loading was 2.0 wt.%, based on the weight of honeycomb. The supported catalysts were aged at 1200°C for 24 h.

A conventional impregnation method was used to synthesize manganese substituted hexaaluminate powders ($15La10Mn75Al_2O_3$). The impregnation of $La(NO_3)_3$ and $Mn(NO_3)_2$ onto γ-Al_2O_3 (S_{BET}=160 m^2 g^{-1}, Sumitomo) was performed in a conventional way. The obtained sample was further dried at 110°C for 12 h and precalcined at 1100°C. The corresponding surface area determined by BET method was 54.2 m^2 g^{-1}. The X-ray diffraction pattern of the sample showed the presence of La–β–Al_2O_3.

The corrugated Fe–Cr alloy (160 cpi, 50 μm, 72.6% Fe, 22% Cr, 4.8% Al, 0.3% Si, 0.3% Y, Goodfellow Cambridge) was dipped into the hexaaluminate slurry containing the precalcined hexaaluminate powder and the peptizing agent, inorganic acids. Then, the corrugated Fr–Cr alloy was dried and heated at 1100°C for 6 h.

Fig. 1 shows an overall scheme of the test rig of the catalytic combustor. A combustion air was supplied from a compressor and controlled by a mass flow controller. The velocity of the combustion air varied between 10 and 25 m/s (500°C). The air was electrically heated to the desired preheating temperature. LNG (CH_4 90.22%, C_2H_6 6.45%, C_3H_8 2.34%, C_4H_{10} 0.99%) was controlled by a mass flow controller and the fuel–air ratio (fuel volume/air volume) ranged from 2.0 to 4.5%. A static mixer was installed downstream of the electric heater so as to make the mixing of fuel and air uniform prior to the inlet of catalyst bed. Uniformity of fuel–air mixing was within ±5% around the mean value at the air velocity of 15 m/s.

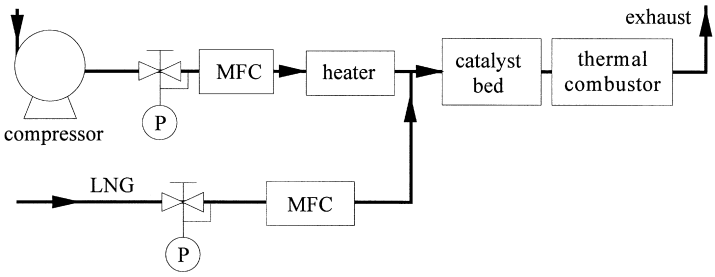

Fig. 1. Schematic diagram of the catalytic combustor.

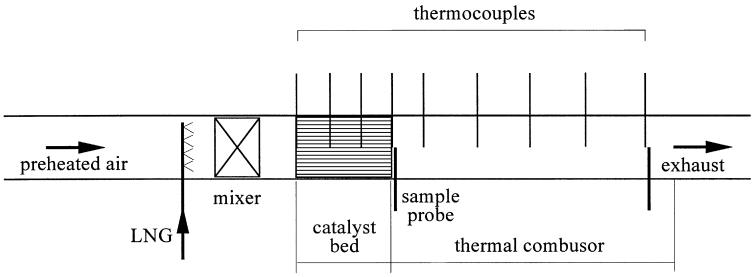

Fig. 2. Catalyst bed and thermal combustor of the catalytic combustor.

A detailed scheme of the catalyst bed and the thermal combustor is shown in Fig. 2. The catalyst bed was 50 mm in diameter and 78 mm in length. The types of the catalyst beds used in this work are illustrated in Table 1. Five types of the catalyst beds were composed of Pd, Pt and La–Mn–hexaaluminate. The thermal combustor was 50 mm in diameter and 1300 mm in length, and had a sight glass at the rear. Both of the catalyst bed and the thermal combustor were insulated with the ceramic fiber of 50 mm thickness.

The temperatures of the catalyst bed were measured with R-type thermocouples of 0.3 mm wire diameter and the thermocouples were attached to the honeycomb using ceramic cement. Temperatures in the thermal combustor were measured with R-type thermocouples of 0.5 mm wire diameter. All the thermocouples within the catalyst bed and the thermal combustor were located along the centerline. The reported temperatures were not corrected for the radiation in the thermocouple.

Gas samples were taken at the exit of the catalyst bed and the end of the thermal combustor. The composition of samples was analyzed on line. CO_2 and CO concentrations were analyzed with NDIR analysis (HORIBA, VIA 510). THC was measured by FID analysis (HORIBA, FIA 510). Water in samples was removed by a sample conditioner before analysis was performed.

Table 1
The catalyst beds tested in the present work

Catalysts beds	Catalysts (diameter, length)
CAT-1	Pd catalyst (50 mm, 78 mm)
CAT-2	Pt catalyst (50 mm, 78 mm)
CAT-3	Pd (50 mm, 52 mm)+Pt (50 mm, 26 mm)
CAT-4	Pd (52 mm)+Hexaaluminate (60 mm)
CAT-5	Pd (26 mm)+Pt (26 mm)+Hexaaluminate (60 mm)

3. Numerical model

For the modeling study of the catalyst bed, a plug flow model with a multi-step homogeneous and heterogeneous chemistry was used. The model was a one-dimensional, steady-state, laminar gaseous reactive flow coupled with the surface reaction. The plug model neglects all radial gradients of variables and also neglects axial diffusive terms, which result in more easy calculation of flow system. Reynold number of the channel flow studied in the present study was lower than 1000, and the flow inside the catalyst bed of the catalytic combustor was treated as a laminar flow. Governing equations of the channel flow are as follows [10].

Continuity equation

$$\frac{\mathrm{d}}{\mathrm{d}X}(\rho u A_\mathrm{c}) = A_\mathrm{p}\sum_{\mathrm{gas}}^{K_\mathrm{g}} \dot{s}_k W_k$$

Momentum equation

$$A_\mathrm{c}\frac{\mathrm{d}P}{\mathrm{d}X} + \rho u A_\mathrm{c}\frac{\mathrm{d}u}{\mathrm{d}X} + A_\mathrm{p}\tfrac{1}{2}\rho u^2 f + u A_\mathrm{p}\sum_{\mathrm{gas}}^{K_\mathrm{g}} \dot{s}_k W_k = 0$$

Species equation

$$\rho u A_\mathrm{c}\frac{\mathrm{d}Y_k}{\mathrm{d}X} + Y_k A_\mathrm{p}\sum_{\mathrm{gas}}^{K_\mathrm{g}} \dot{s}_k W_k = W_k(A_\mathrm{p}\dot{s}_k + A_\mathrm{c}\dot{\omega}_k)$$

$$(k = 1, \ldots, K_\mathrm{g})$$

Energy equation

$$\rho u A_c \left(\sum_{gas}^{K_g} h_k + \frac{dY_k}{dX} + \overline{C_p} \frac{dT}{dX} + u \frac{du}{dX} \right) + \left(\sum_{gas}^{K_g} h_k Y_k + \frac{1}{2} u^2 \right) A_p \sum_{gas}^{K_g} \dot{s}_k W_k = -A_p \sum_{bulk}^{K_b} \dot{b}_k W_k h_k$$

where ρ is the density, u the axial velocity, A_c the cross sectional area of the channel, A_p the internal surface area of the channel, W_k the molecular weight of species, $\dot{s}_k$ the molar production rate of species by surface reaction, P the pressure, f the friction coefficient, Y_k the mass fraction of species, $\dot{\omega}_k$ the molar production rate of gas reaction, h_k the specific enthalpy of species, T the temperature, $\dot{b}_k$ the molar production rate of bulk solid species by surface reaction, K_g the species of gas phases, K_b the bulk species on a catalytic surface, and $\overline{C_p}$ the mean heat capacity per unit mass of the gas.

To solve the governing equations, PLUG software [10] was used. Gas phase reaction mechanism and kinetic data were taken from GRI-Mech Version 1.2 [11]. The gas phase chemical reaction rates were obtained by CHEMKIN [12] software. For surface chemistry, reaction mechanisms [13–15] published on CH_4 oxidation over platinum were evaluated and the most accurate reaction mechanism was employed for parametric investigation of the catalyst bed. The surface chemical reaction rates were obtained from SURFACE CHEMKIN [16].

Modeling of the thermal combustor was carried out using a one-dimensional multi-step homogeneous chemistry and PREMIX software [17]. The program accounts for finite-rate gas phase kinetics and multi-component molecular transport. Gas phase reaction mechanism and kinetic data were taken from GRI-Mech Version 1.2 [11], the same model as in the catalyst bed. The transport properties were calculated using TRANSPORT [18] software. Results calculated from the catalyst bed were used as the input conditions of the thermal combustor to evaluate effects of surface reaction on homogeneous reaction in the thermal combustor.

4. Results and discussion

4.1. Experimental

Reaction in the catalyst bed starts when the air–fuel mixture is heated to the required temperature for surface reaction. In the catalytic combustor for gas turbines, the surface ignition temperature of catalysts should be less than the compressor discharge temperature. If the surface ignition temperature is higher than this air temperature, the combustion air must be heated, typically by a burner upstream of the catalyst bed.

First, characteristics on the surface ignition of catalyst beds were investigated. Temperatures within the catalyst bed were measured as a function of the preheating temperature of mixture. The preheating temperature was ramped at a rate of 5°C/min beginning at 350°C. Fig. 3 shows wall temperatures of the catalyst bed measured for three types of catalysts (CAT-1, CAT-2 and CAT-3). In CAT-1 composed of Pd catalyst, when the preheating temperature reached 480°C, the exit temperature of the catalyst bed ($T_{c,78}$) increased rapidly from about 500 to 780°C, indicating that the surface reaction in the catalyst bed has been initiated. The preheating temperature at which the surface reaction ignites, is called LOT (light-off temperature) of surface reaction.

As can be seen in Table 2, light-off temperatures of CAT-1 and CAT-3 are almost same and the light-off temperature of CAT-2 is higher than that of CAT-1 and CAT-2. The light-off temperature was defined as the preheating temperature when the exit temperature ($T_{c,78}$) of the catalyst bed begins increasing rapidly apart from the preheating temperature. These results demonstrate that Pd catalyst is much better in the

Table 2
Light-off temperatures of each catalyst bed. (mixture velocity: 11.4 m/s, fuel–air ratio: 2.94%)

Catalyst bed	CAT-1	CAT-2	CAT-3
Catalysts (length, mm)	Pd (78)	Pt (78)	Pd (52)+Pt (26)
Light-off temperature (°C)	483	595	475
Maximum operating temperature[a]	708	608	585

[a] Preheating temperature at which the temperature of the catalyst bed reaches 900°C.

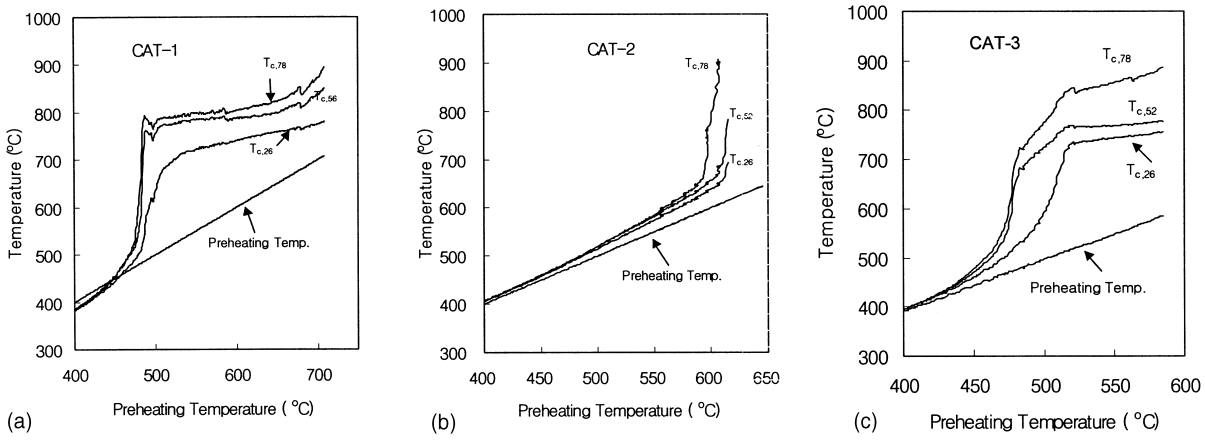

Fig. 3. Temperatures of the catalyst bed according to preheating temperatures (mixture velocity: 11.49 m/s (500°C), fuel–air ratio: 3.49%): (a) CAT-1; (b) CAT-2; (c) CAT-3. In the figure, a subscripted number represents the distance from the inlet of the catalyst bed and a subscript "c" represents the catalyst bed.

catalyst activity than Pt catalyst. Comparing CAT-2 with CAT-3, the light-off temperature of the catalyst bed depends chiefly on catalysts located in the first stage of the catalyst bed. It is supported by the result that the light-off temperature of CAT-3 is the same as that of CAT-1 even though CAT-3 is composed of Pd and Pt catalysts.

After the ignition of surface reaction, the behavior of the catalyst bed was quite different depending on the kinds of catalysts. In CAT-1, temperatures of the catalyst bed rose only slightly when the preheating temperature increased above light-off temperature. Wall temperatures of CAT-1 stayed at almost the constant temperature (780–790°C) after surface ignition, irrespective of the increase of the preheating temperature from 490 to 600°C. However, temperatures of the catalyst bed of CAT-2 increased rapidly after surface ignition. These different behaviors are caused by the spontaneous decomposition of PdO at temperatures near 800°C.

Farrauto et al. [19] reported that the Pd catalyst is in the form of PdO at room temperature and changes from PdO to metallic Pd at 750–800°C, at atmospheric pressure. When wall temperatures of Pd catalyst reach 800°C, PdO decomposes to metallic Pd. Because the catalytic activity of metallic Pd is much lower than that of PdO, the catalytic activity rapidly decreases. This change in the catalytic activity causes the wall temperatures of CAT-1 to remain almost constant. The decomposition of PdO to metallic Pd is called the self-regulation characteristics of Pd catalyst [6].

The temperature distribution along the catalyst bed was also measured for each catalyst as shown in Fig. 4. Temperatures in CAT-1 increased rapidly in the front of the catalyst bed as soon as surface reaction started, and reached a maximum in the middle. Temperatures in the rear of the catalyst bed changed slightly from the maximum of 790°C. However, temperature distributions in CAT-2 showed quite a different pattern from CAT-1. As the preheating temperature increased up to the surface ignition point, only the temperatures in the rear part of the catalyst bed increased rapidly and those of the front remained at the level of preheating temperature. As the preheating temperature further increased to 625°C, temperatures in the rear part increased more rapidly, and those in the front increased slowly. These differences between CAT-1 and CAT-2 are due to catalytic activities of each catalyst. The Pd catalyst has high catalytic activity and self-regulation characteristics above 800°C. However, the Pt catalyst has lower catalytic activity as compared with Pd catalyst and no self-regulation. Meanwhile, CAT-3 showed combined characteristics of CAT-1 and CAT-2. The front part of the bed behaved as the CAT-1 of Pd catalyst and the back part of the bed as the CAT-2 of Pt catalyst.

We also tested a La–Mn–hexaaluminate high temperature catalyst located downstream of a Pd and Pd/Pt catalyst, as shown in Fig. 5. CAT-4 consists of

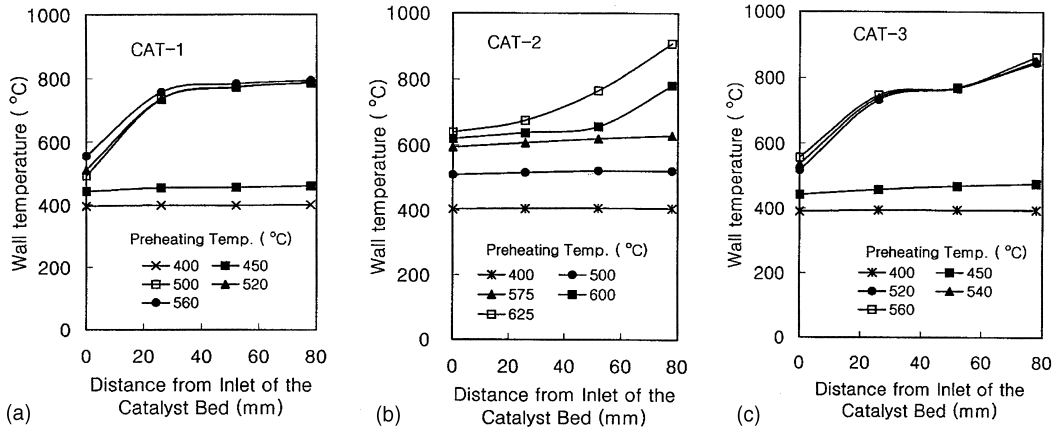

Fig. 4. Temperature distributions along the catalyst bed (mixture velocity: 11.49 m/s, fuel–air ratio: 3.49%): (a) CAT-1; (b) CAT-2; (c) CAT-3.

Pd (the first stage, 52 mm) and hexaaluminate (the second stage, 60 mm). In Fig. 5(a), $T_{c,26}$ and $T_{c,50}$ represent temperatures of Pd catalyst in CAT-4, and $T_{c,82}$ and $T_{c,112}$ are temperatures of hexaaluminate. As the preheating temperature was raised to 397°C, surface ignition took place and the exit temperature of Pd catalyst ($T_{c,50}$) increased to 820°C. Hexaaluminate also ignited and its exit temperature ($T_{c,112}$) increased to 1200°C. The conversion of LNG-air mixture at the exit of the hexaaluminate catalyst bed was about 50%. As preheating temperature was further raised to 482°C, the exit temperature of Pd catalyst increased over 1000°C, and the operation was shut to protect the Pd catalyst.

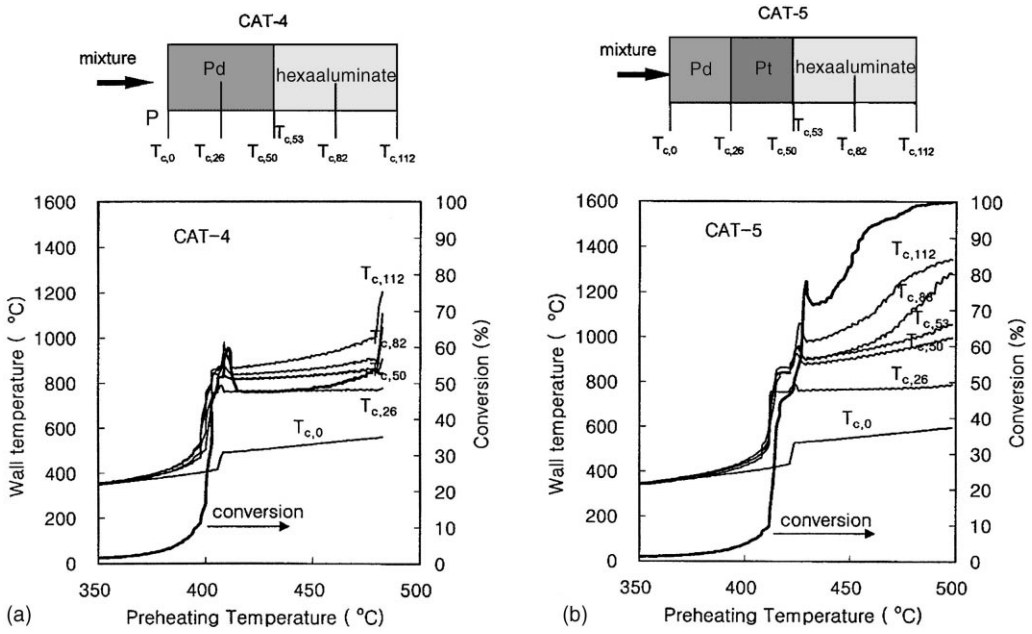

Fig. 5. Temperatures of the catalyst bed in CAT-4 and CAT-5 (mixture velocity: 11.49 m/s, fuel–air ratio: 3.49%): (a) CAT-4; (b) CAT-5.

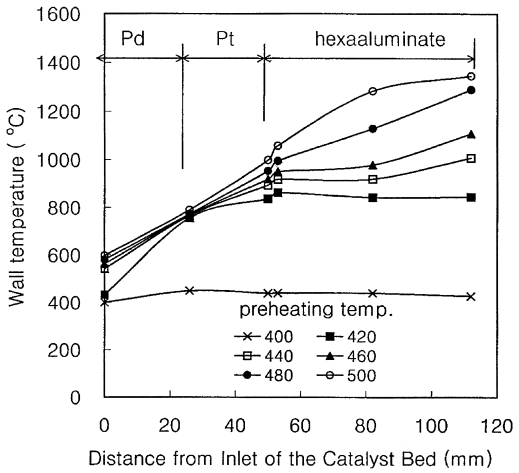

Fig. 6. Temperature distributions along the catalyst bed of CAT-5 (mixture velocity: 11.49 m/s, fuel–air ratio: 3.49).

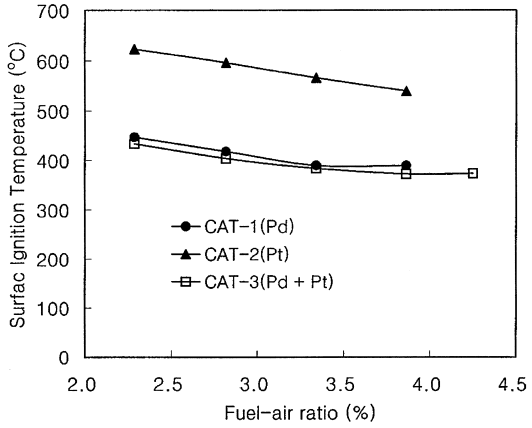

Fig. 7. Light-off temperatures of each catalyst bed as a function of the fuel–air ratio at mixture velocity of 11.49 m/s.

Fig. 5(b) represents the results of CAT-5 which is composed of Pd (the first stage, 26 mm), Pt (the second stage, 26 mm) and hexaaluminate (the final stage, 60 mm). The overall trends of CAT-5 were quite a little different from CAT-4. As the preheating temperature was raised above the LOT, temperatures of Pt and hexaaluminate increased steadily. Homogeneous reaction occurred within the catalyst bed when preheating temperature increased to 427°C, with the conversion increasing quickly from 46 to 72%. The preheating temperature was limited for the temperature of the catalyst bed to be kept below 1400°C. When the preheating temperature was further elevated to 488°C, conversion was complete, and the CO level was 232 ppm with THC of 7 ppm.

Temperature distributions in the catalyst bed of CAT-5 were measured as illustrated in Fig. 6. When the preheating temperature was 420°C, little conversion took place in any of the catalyst beds. As the preheating temperature was raised to 440°C, the exit temperature of the hexaaluminate increased. When preheating temperature was further elevated to 500°C, the exit temperature of the hexaaluminte increased to 1345°C, the adiabatic flame temperature of the mixture. However, the temperatures of the Pd and Pt beds remained below 1000°C. The operation was then shut down to protect the catalyst bed.

Fig. 7 illustrates the surface ignition temperatures of each catalyst bed as a function of the fuel–air ratio. Light-off temperature of CAT-1 decreased from 450 to 390°C as the fuel–air ratio increased from 2.3 to 4.3% and that of CAT-2 decreased from 623 to 530°C for the same increase in fuel–air ratio. As a whole, the surface ignition temperature decreased as the fuel–air ratio of the mixture increased. This can be explained by the fact that the rate of methane oxidation over Pd catalyst is 0.45–0.8 order in CH_4 concentration [20]. Comparing surface ignition temperatures of each catalyst bed, those of CAT-2 were about 170°C higher than those of CAT-1, and CAT-1 showed nearly the same LOT as CAT-3. It demonstrates that the Pd catalyst is much more active for LNG combustion than the Pt catalyst, and that the ignition temperature of the multi-stage catalyst bed is mainly governed by the most active catalyst. As a result, to lower the surface ignition temperature of the catalyst bed, it is desirable to place the most active catalysts in the first stage of the multi-stage catalyst bed.

In a CST combustor, a partially combusted mixture enters the thermal combustor and is completely combusted homogeneously. Therefore, flame ignition and emissions in the thermal combustor are very important. In this study, flame ignition in thermal combustor for each catalyst bed was investigated at various operation conditions and effects of catalyst beds and operating parameters on flame ignition were analyzed. Fig. 8 represents temperature distributions in the thermal combustor of CAT-3 as a function of preheating temperature. When preheating temperature was set

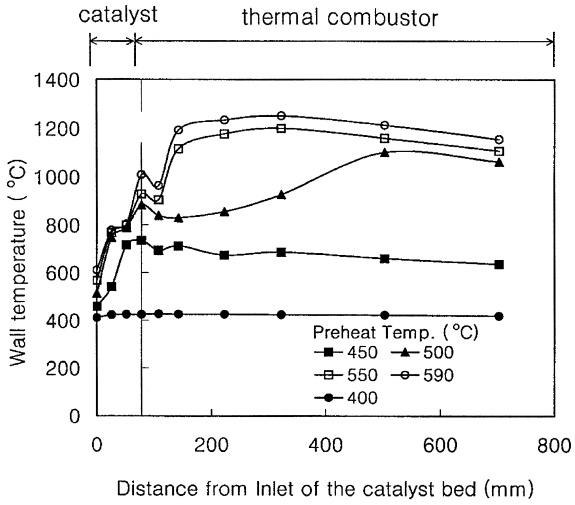

Fig. 8. Temperature distributions in the thermal combustor of CAT-3 (mixture velocity: 11.44 m/s, fuel–air ratio: 2.94%).

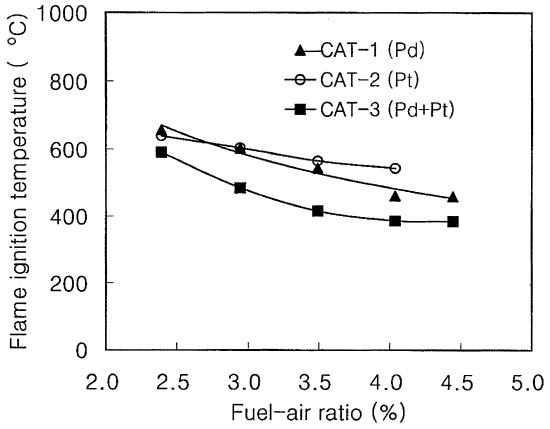

Fig. 9. Flame ignition temperatures of each catalyst bed as a function of the fuel–air ratio (mixture velocity: 11.49 m/s).

to 400°C at the mixture velocity of 11.4 m/s and the fuel–air ratio of 2.94%, both the catalyst bed and the thermal combustor were not ignited. As the preheating temperature was raised to 450°C, the surface reaction in the catalyst bed was ignited and its exit temperature ($T_{c,78}$) rose to 735°C, whereas the thermal combustion was not yet ignited. When preheating temperature increased above 500°C, both of surface reaction and thermal combustion were ignited. These results show that homogeneous reaction in the thermal combustor of CST combustor is initiated only under limited operating conditions.

Based on the results of Fig. 8, parametric investigations on homogeneous ignition in each catalyst bed were performed. Fig. 9 is the plot of preheating temperatures for flame ignition in each catalyst bed as a function of fuel–air ratio. The preheating temperature for flame ignition in CAT-1 was 657°C when the fuel–air ratio was 2.39%. It decreased to 459°C as the fuel–air ratio increased to 4.44%. The preheating temperature for flame ignition generally decreased as the fuel–air ratio increased.

Among three types of catalyst beds, CAT-3 had the lowest preheating temperature for flame ignition, and the flame ignition temperature in CAT-1 was higher than in CAT-3. Considering that CAT-1 had nearly the same surface ignition temperature as CAT-3, these results appear contradictory. However, this can be explained by the fact that Pd catalyst has self-regulation characteristics and its wall temperature remains below 800°C. The wall temperatures of Pt catalyst increase steadily with increasing preheating temperature so that the exit temperature of Pt catalyst easily reaches the temperature needed to initiate the homogeneous reaction. This result suggests that the surface ignition temperature can be lowered using the Pd catalyst in the first stage and the preheating temperature needed for flame ignition in the thermal combustor can be lowered using the Pt catalyst in the second stage.

4.2. Modeling

Multi-step surface reaction mechanism of CH_4 oxidation over Pt catalysts was first reported by Deutschmann et al. [21], who used them to model methane oxidation on a platinum foil. Thereafter, Bond et al. [14] reported another elementary surface reaction mechanism of CH_4 oxidation over Pt catalysts. Bond showed that conversions calculated in a honeycomb monolith were underestimated as compared with experimental results. Recently, Chou et al. [15] presented an updated surface reaction mechanism, which revised the reaction mechanism proposed by Bond. This multi-step surface reaction mechanism was shown to agree well with experimental results measured in a honeycomb monolith.

In the present work, three sets of multi-step elementary surface reactions were evaluated on a honeycomb

Table 3
Surface reaction mechanism of methane oxidation on platinum

	Reaction[a]	A[b]	S[c]	β	Ea[d]
Adsorption					
A1	O_2+2PT(*)⇒2O(*)+2PT(B)		0.003	0.0	0.00
A2	CH_4+2PT(*)⇒CH_3(*)+H(*)+2PT(B)		0.150	0.0	27.00
A3	CH_4+O(*)+PT(*)⇒CH_3(*)+OH(*)+PT(B)		0.430	0.0	59.20
A4	CO+PT(*)⇒CO(*)+PT(B)		0.840	0.0	0.00
A5	H_2+2PT(*)⇒H(*)+H(*)+2PT(B)		0.046	0.0	0.00
A6	OH+PT(*)⇒OH(*)+PT(B)		1.000	0.0	0.00
A7	H_2O+PT(*)⇒H_2O(*)+PT(B)		0.500	0.0	0.00
Surface reaction					
S1	CH_3(*)+PT(*)⇒CH_2(*)+H(*)+PT(B)	1.0E+21		0.0	20.00
S2	CH_2(*)+PT(*)⇒CH(*)+H(*)+PT(B)	1.0E+21		0.0	20.00
S3	CH(*)+PT(*)⇒C(*)+H(*)+PT(B)	1.0E+21		0.0	20.00
S4	H(*)+O(*)+PT(B)⇒OH(*)+PT(*)	1.0E+19		0.0	10.50
S5	OH(*)+PT(*)⇒H(*)+O(*)+PT(B)	1.0E+12		0.0	20.80
S6	H(*)+OH(*)+PT(B)⇒$H_2$0(*)+PT(*)	l.0E+21		0.0	62.50
S7	2OH(*)⇒H_2O(*)+O(*)	1.0E+20		0.0	51.25
S8	H_2O(*)+PT(*)⇒OH(*)+H(*)+PT(B)	l.8E+13		0.0	54.20
S9	C(*)+O(*)+PT(B)⇒CO(*)+PT(*)	5.0E+20		0.0	62.50
S10	CO(*)+PT(*)⇒C(*)+O(*)+PT(B)	1.0E+13		0.0	156.50
S11	CO(*)+O(*)+2PT(B)⇒CO_2+2PT(*)	4.0E+20		0.0	100.80
Desorption					
D1	2O(*)+2PT(B)⇒O_2+2PT(*)	l.0E+21		0.0	216.00
D2	CO(*)+PT(B)⇒CO+PT(*)	8.5E+12		0.0	152.50
D3	2H(*)+2PT(B)⇒H_2+2PT(*)	5.0E+20		0.0	67.40
D4	OH(*)+PT(B)⇒OH+PT(*)	1.5E+13		0.0	192.80
D5	H_2O(*)+PT(B)⇒H_2O+PT(*)	1.0E+13		0.0	45.00

[a] The kinetic constant of the ith reaction is expressed in the modified Arrhenius form $k_i = AT^{\beta}\exp(-E_a/R_uT)$.
[b] Pre-exponential factor in units of cm-mol-s.
[c] Sticking coefficient.
[d] Activation energy (kJ mol^{-1}).

monolith with a Pt catalyst (Table 3). Experimental results of CAT-2 were used to evaluate the multi-step elementary reaction mechanisms of methane oxidation over Pt. Fig. 10 illustrates their calculated conversion of the mixture together with measured values. The experimental results of Fig. 10 were measured using LNG (CH_4: 90.22%, C_2H_6: 6.45%, C_3H_8: 2.34%, C_4H_{10}: 0.99%), not pure methane. However, because C_2H_6, C_3H_8 and C_4H_{10} could not be used in the calculation of gas reaction rates and surface reaction rates, the compositions of LNG was artificially corrected to 100% CH_4 for numerical calculation.

The case using Deutschmann's surface chemistry shows quite a difference between predicted and measured conversions, and thus Deutschmann's surface chemistry is considered not to be proper for the simulation of honeycomb catalyst used in the present study. Prediction by the use of Bond's surface chemistry agrees better with measured results. At inlet temperature less than 620°C, predicted conversions are higher than measured conversions, whereas at inlet temperature above 620°C the calculated conversion is lower than the experimental result. Specially, measured conversion increases rapidly at the inlet temperature above 630°C, but numerical calculation using Bond's surface chemistry does not predict this rapid increase of conversion.

Calculation using Chou's surface chemistry was revealed to agree best with experimental results even though it predicts a little less than the measured conversion. It also shows the good prediction even in the region that the conversion is rapidly increasing at the inlet temperature over 630°C. Surface chemistry proposed by Chou seems to more accurately model the

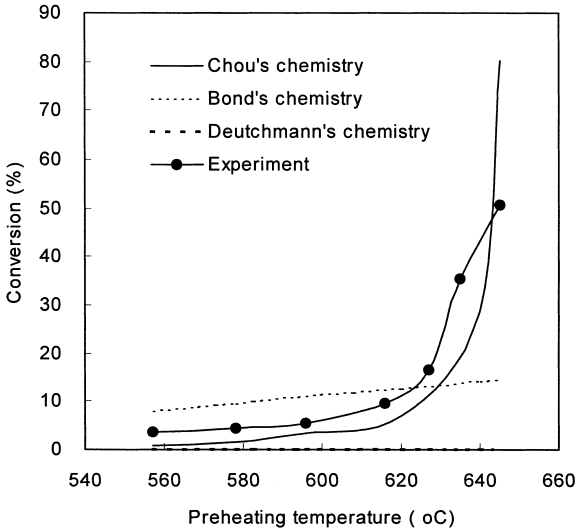

Fig. 10. Comparison between measured and calculated conversions using three kinds of surface chemistry (channel dimension: 78 mm in length, 1.20 mm in hydraulic diameter, fuel–air ratio: 2.94%, inlet velocity: 16.7 m/s).

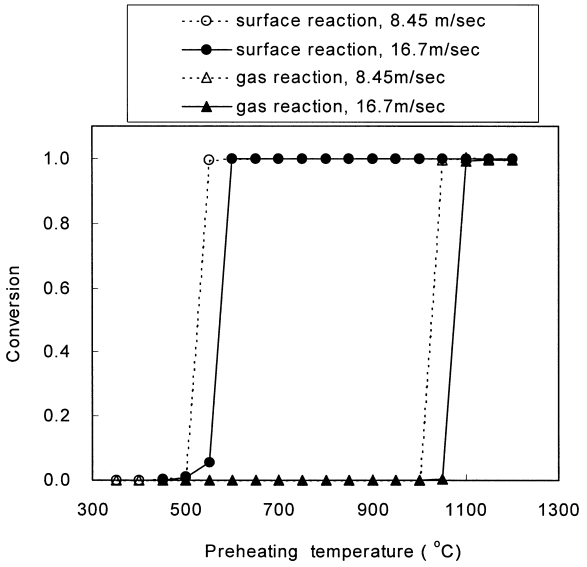

Fig. 11. Comparison between ignition temperatures of gas reaction and catalytic surface reaction (channel dimension: 10 cm length, fuel–air ratio: 4.0%).

honeycomb monolith with Pt catalyst. Therefore all calculations of the catalyst bed were conducted using Chou's surface chemistry.

Ignition temperatures of the mixture in the catalyst bed were investigated for two cases — gas reaction and catalytic surface reaction. Fig. 11 represents conversions of the mixture as a function of the preheating temperature for the channel of 1.27 mm hydraulic diameter and 10 cm length at the fuel–air ratio of 4.0%. In the case of the catalytic surface reaction, the reaction begins when the inlet temperature increases to 500°C at the mixture velocity of 16.7 m/s. Then its conversion reaches 100% when the inlet temperature increases to 600°C. In the case of gas reaction, the reaction starts when the inlet temperature is 1050°C at the mixture velocity of 16.7 m/s and its conversion becomes 100% at 1100°C. Comparing ignition temperatures between two cases, the ignition temperature of surface reaction shows 450°C lower than that of gas reaction. This indicates that the ignition temperature of catalytic surface reaction is much lower than that of gas reaction.

When flame is initiated by the surface reaction, it is expected that the flame supported by catalytic reaction has different behaviors from the flame without catalytic reaction. Thus, the flame speed of mixture supported by catalytic reaction was examined. Fig. 12 shows flame speeds calculated according to the degree of surface reaction.

The flame speed of mixture without surface reaction was calculated to 47 cm/s at the fuel–air ratio of

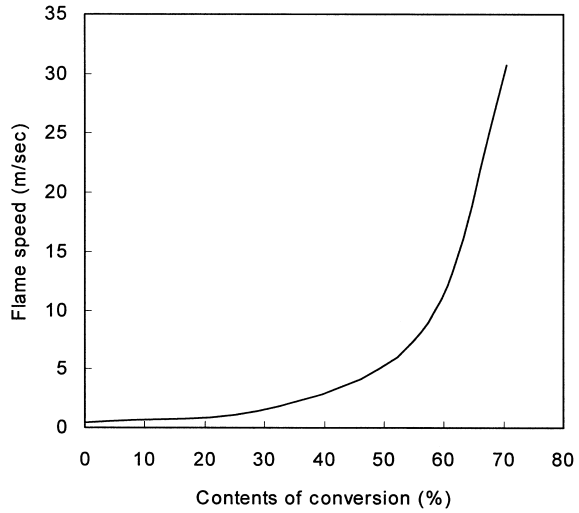

Fig. 12. Variation of flame speed according to the degree of surface reaction inside the catalytic channel (inlet temperature: 645°C, fuel–air ratio: 2.94%).

2.94%, the mixture velocity of 16.7 m/s and the inlet temperature of 645°C. As the degree of conversion by surface reaction becomes 33%, the flame speed increases to 1.9 m/s, four times as high as the flame speed of mixture without catalytic reaction. This increase of flame speed is caused by the rise of mixture temperature through surface reaction and intermediates diffused from catalytic reaction. In the flame combustion supported by surface reaction, the mixture temperature rises due to heats released from catalytic surface and the mixture includes some intermediates generated from catalytic reaction. When the amount of conversion further increases to 57%, flame speed increases to 9.0 m/s, 19 times as high as the flame speed without catalytic reaction. The flame speed increases exponentially with the degree of conversion by surface reaction.

The increase of flame speed is very important from the viewpoint of flame stability. The faster the flame speed is, the easier the flame stability becomes. For example, a lean combustion, which has been developed as one of low-NO_x technologies, has a problem that the flame becomes unstable as the fuel concentration goes to near the lean limit of the mixture. This is because the flame speed decreases as the fuel concentration becomes lean. If the flame combustion is supported by catalytic reaction, the flame speed increases and the flame stability can be improved. In fact, in the catalytically stabilized combustion whose inlet velocities are usually 10–30 m/s, flame can be kept safely without an additional flame holder.

It is also expected that the flame combustion with surface reaction produces less CO emission, one of main pollutants exhausted from combustors. Fig. 13 illustrates predicted CO mole fractions in the catalytic combustor. The numerical evaluation of CO emission was conducted for three cases — catalytic reaction only, gas reaction only, and gas reaction combined with catalytic reaction. The case of only gas reaction shows more CO fraction than other two cases. The case of only surface reaction reveals the least CO fraction. Maximum CO mole fraction of only gas reaction is 5.0×10^{4} times as much as that of only surface reaction.

The case of only surface reaction shows the least CO fraction and CO fraction diminishes fast below 1.0×10^{-10} after the peak. This implies that combustors with surface reaction exhaust the least CO emission. The minimum CO fraction of only gas reaction

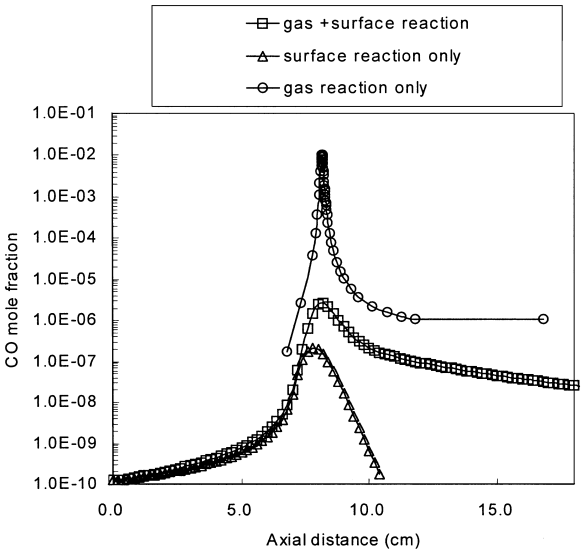

Fig. 13. Predicted CO mole fraction in three cases — surface reaction only, gas reaction only, and surface reaction coupled with gas reaction in the catalytic channel (inlet temperature: 645°C, fuel–air ratio: 2.94%, inlet velocity: 16.7 m/s).

is 1.1×10^{-6}, the largest value as compared to the other two cases. The large difference in CO fraction between only surface reaction and only gas reaction is caused by the fact that catalyst surface plays a role of absorption of CO species.

5. Conclusions

Test results showed that the surface ignition temperature is lowered in the Pd catalyst, and the flame ignition temperature in the thermal combustor is lowered in the Pt catalyst. One of best ways to lower the preheating temperature for surface ignition in the catalyst bed and simultaneously lower the preheating temperature for flame ignition in the thermal combustor is to locate Pd catalyst in the first stage of the catalyst bed and Pt catalyst in the second stage.

The numerical simulation showed that the flame speed of the mixture supported by catalytic surface reaction is much raised as compared to mixture without a catalytic combustion. The flame speed of the mixture was calculated 47 cm/s when its combustion is not supported by surface reaction. However, when the conversion of the mixture by surface reaction is 57%,

the flame speed increases to 9.0 m/s, 19 times as high as the flame speed without catalytic reaction.

CO mole fractions were numerically analyzed for three cases — gas reaction, surface reaction, and gas reaction coupled with surface reaction. The case of only gas reaction produced the most CO emission and the case of only surface reaction produced the lest CO emission. This result shows that the catalytically stabilized combustor may produce less CO emission as compared to the conventional combustor of flame combustion.

Acknowledgements

We would like to thank the Ministry of Science and Technology (Korea) for providing financial support.

References

[1] H. Sadamori, T. Tanioka, T. Matsuhisa, Catal. Today 26 (1995) 337–344.
[2] T. Furuya, K. Sasaki, Y. Hanakata, T. Ohhashi, M. Yamada, T. Tsuchiya, Y. Furuse, Catal. Today 26 (1995) 345–350.
[3] R.A. Dalla Betta, J.C. Schlatter, S.G. Nickolas, D.A. Smith, ASME, 95-GT-65, 1995.
[4] R.A. Dalla Betta, J.C. Schlatter, S.G. Nickolas, M.B. Cutrone, K.W. Beebe, Y. Furuse, T. Tsuchiya, Trans. ASME 119 (1997) 844–851.
[5] W.C. Pfefferle, J. Energy 2 (3) (1978) 142–146.
[6] T.W. Griffin, W. Weisenstein, V. Scherer, M. Fowles, Combust. Flame 101 (1995) 81–90.
[7] S. Hyayashi, H. Yamada, K. Shimodaira, Catal. Today 26 (1995) 319–327.
[8] L.M. Quick, S. Kamitomai, Catal. Today 26 (1995) 303–308.
[9] N. Vortmeyer, M. Valk, G. Kappler, J. Eng. Gas Turbines Power 118 (1996) 61–64.
[10] R.S. Larson, Sandia National Laboratories, Livermore, CA, SAND 96-8211, 1996.
[11] GRI-Mech Version 1.2, 1994. http://diesel.fsc.psu.edu/~gri_mech.
[12] R.J. Kee, F.M. Rupley, E. Meeks, J.A. Miller, Sandia National Laboratories, Livermore, CA, SAND 96-8216, 1996.
[13] O. Deutschmann, R. Schmidt, F. Behrendt, J. Warnatz, Proceedings of the 26th International Symposium on Combustion, The Combustion Institute, Pittsburgh, 1996, pp. 1747–1754.
[14] T.C. Bond, R.A. Noguchi, C.-P. Chou, R.K. Mongia, J.-Y. Chen, R.W. Dibble, Proceedings of the 26th International Symposium on Combustion, The Combustion Institute, Pittsburgh, 1996, pp. 1771–1778.
[15] C.-P. Chou, J.-Y. Chen, G.H. Evans, W.S. Winters, Numerical studies of methane catalytic combustion inside a monolith honeycomb reactor using multi-step surface reaction, Combust. Sci. Technol., to be submitted.
[16] M.E. Coltrin, R.J. Kee, F.M. Rupley, E. Meeks, Sandia National Laboratories, Livermore, CA, SAND 96-8217, 1996.
[17] R.J. Kee, J.F. Grcar, M.D. Smooke, J.A. Miller, E. Meeks, Sandia National Laboratories, Livermore, CA, 1998.
[18] R.J. Kee, G. Ddixon-Lewis, J. Warnatz, M.E. Coltrin, J.A. Miller, H.K. Moffat, Sandia National Laboratories, Livermore, CA, SAND 86-8246B.
[19] R.J. Farrauto, M.C. Hobson, T. Kennelly, E.M. Waterman, Appl. Catal. A 81 (1992) 227–237.
[20] J.H. Lee, D.L. Trimm, Fuel Processing Technol. 42 (1995) 339–359.
[21] O. Deutschmann, F. Behrendt, J. Warnatz, Catal. Today 21 (1994) 461–470.